Title	Formation of an embryonic supermassive star in the first galaxy
Author(s)	Inayoshi, Kohei; Omukai, Kazuyuki; Tasker, Elizabeth
Citation	Monthly notices of the Royal Astronomical Society, 445(1), L109-L113 https://doi.org/10.1093/mnrasl/slu151
Issue Date	2014-11-21
Doc URL	http://hdl.handle.net/2115/57652
Rights	This article has been accepted for publication in Monthly Notices of the Royal Astronomical Society ©: 2014 The Authors Published by Oxford University Press on behalf of The Royal Astronomical Society. All rights reserved.
Type	article
File Information	MNRAS_445_L109-.pdf

Monthly Notices
of the
ROYAL ASTRONOMICAL SOCIETY

MNRASL **445,** L109–L113 (2014) doi:10.1093/mnrasl/slu151

Formation of an embryonic supermassive star in the first galaxy

Kohei Inayoshi,[1,2]★ Kazuyuki Omukai[3] and Elizabeth Tasker[4]

[1]*Department of Physics, Graduate School of Science, Kyoto University, Kyoto 606-8502, Japan*
[2]*Department of Astronomy, Columbia University, 550 West 120th Street, New York, NY 10027, USA*
[3]*Astronomical Institute, Tohoku University, Sendai 980-8578, Japan*
[4]*Department of Physics, Faculty of Science, Hokkaido University, Sapporo 060-0810, Japan*

Accepted 2014 September 8. Received 2014 September 8; in original form 2014 April 17

ABSTRACT

We studied the gravitational collapse of a warm ($\sim$8000 K) primordial-gas cloud as a candidate progenitor for a supermassive star (SMS; $\gtrsim 10^5$ M$_\odot$) using a three-dimensional hydrodynamical simulation including all the relevant cooling processes of both H$_2$ and H, which can potentially induce cloud fragmentation. This is the first simulation of this kind to resolve protostar formation. We find that from a weakly turbulent initial condition, the cloud undergoes runaway collapse without a major episode of fragmentation. Although the H$_2$ fraction jumps by a large factor via the three-body reaction at $\sim 10^{-13}$ g cm^{-3}, its cooling remains inefficient due to the optical thickness, and the temperature remains $\gtrsim$3000 K. When the central core of the cloud becomes opaque to continuum radiation at $\sim 10^{-8}$ g cm^{-3}, a hydrostatic protostar with $\simeq$0.2 M$_\odot$ is formed. The protostar grows to the mass $\simeq$1 M$_\odot$ and the radius $\simeq$2 au within $\sim$1 yr via rapid accretion of dense filamentary flows. With high accretion rate, $\sim$2 M$_\odot$ yr^{-1}, the protostar is expected to turn into an SMS within its lifetime, eventually collapsing to a seed for the supermassive black hole observed in the early Universe at $z \sim 7$.

Key words: stars: formation – quasars: supermassive black holes – cosmology: theory – dark ages, reionization, first stars.

1 INTRODUCTION

Recent observations reveal the existence of supermassive black holes (SMBHs) with masses $\gtrsim 10^9$ M$_\odot$ as early as redshift $z \gtrsim 7$ (e.g. Fan 2006; Mortlock et al. 2011). Their very existence puts a strong constraint on the origin and formation pathway of SMBHs, since the time required to form such massive objects from stellar-mass seed BHs ($\sim$100 M$_\odot$) exceeds the then Hubble time. As a solution to this conundrum, the formation from massive seed BHs originating in the collapse of supermassive stars (SMSs; $\gtrsim 10^5$ M$_\odot$) has been suggested (e.g. Begelman, Volonteri & Rees 2006). Seed BHs formed in this way are expected to grow to $\gtrsim 10^9$ M$_\odot$ by $z \sim 7$ via subsequent gas accretion (Di Matteo et al. 2012).

SMSs can be formed within primordial-gas clouds in massive haloes with virial temperature $\gtrsim 10^4$ K, providing that H$_2$ cooling is prohibited throughout the protostellar collapse. Without this latter constraint, the gas would rapidly cool via H$_2$ and fragment into smaller pieces. H$_2$ has to therefore be dissociated e.g. via the photodissociation by far-ultraviolet (FUV) radiation from nearby star-forming galaxies (Omukai 2001; Bromm & Loeb 2003; Shang, Bryan & Haiman 2010; Inayoshi & Omukai 2011) or the collisional dissociation in the shocked gas (Inayoshi & Omukai 2012). This in place, the cloud can collapse almost isothermally at $\sim$8000 K solely by the H-atomic cooling. Previous numerical studies (e.g. Bromm & Loeb 2003; Wise, Turk & Abel 2008; Shang, Bryan & Haiman 2010) have implied that such a cloud collapses monolithically without efficient fragmentation. After a protostar is formed at the centre, it then grows rapidly to an SMS via accretion from the envelope at a rate $\gtrsim$0.1 M$_\odot$ yr^{-1}. Under such a high accretion rate, its growth is not hindered either by strong radiative feedback (Hosokawa, Omukai & Yorke 2012; Hosokawa et al. 2013) or by mass-loss due to stellar pulsations (Inayoshi, Hosokawa & Omukai 2013).

So far, however, most studies (e.g. Regan & Haehnelt 2009; Choi, Shlosman & Begelman 2013; Latif et al. 2013b) have utilized several simplifying assumptions in studying the fragmentation process, e.g. turning off the H$_2$ cooling, adopting optically thin treatment of Lyα cooling, or using insufficient chemical networks that neglect the H$_2$ formation. Yet the efficiency of fragmentation depends strongly on the thermal evolution determined by the cooling processes and chemical reactions. As a result, it still remains unresolved whether the cloud fragments during the isothermal collapse at $\sim$8000 K before forming the protostar. In this Letter, we use a three-dimensional hydrodynamical simulation to study the gravitational collapse of a turbulent primordial-gas cloud with mass $\gtrsim 10^5$ M$_\odot$. We follow the evolution until the formation of the protostar, including all relevant processes required for examining possible fragmentation during this collapse. Among these, the H$_2$-line cooling is of primary importance due to its ability to rapidly drop the temperature via thermal

---

★ E-mail: inayoshi@astro.columbia.edu

Published by Oxford University Press on behalf of the Royal Astronomical Society

instability if the gravitational collapse is delayed, a process possible due to turbulence generated during the virialization of the halo. If the thermal instability occurs, the cloud can fragment into many smaller mass clumps instead of forming a single SMS. We therefore simulate the collapse to determine the likelihood of the outcome being a monolithic collapse to a single star or fragmentation into a binary or multiple member system.

2 METHODOLOGY

We performed a three-dimensional hydrodynamical simulation of the gravitational collapse of a primordial-gas cloud using the adaptive mesh refinement code, ENZO (Bryan et al. 2014). Our main purpose is to investigate the gas dynamics over a wide range of the densities ($10^{-21} \lesssim \rho \lesssim 10^{-7}$ g cm^{-3}). The cloud initially has a spherically symmetric density profile enhanced by a factor $f(=1.6)$ above the critical Bonnor–Ebert (BE) distribution, an isothermal sphere embedded in a pressurized medium and supported in marginal hydrostatic equilibrium against gravitational collapse. According to cosmological simulations (e.g. Wise et al. 2008), at the centre of a first galaxy with virial temperature $\gtrsim 10^4$ K, forming in an environment where the H_2 formation is suppressed, a warm ($T \sim 8000$ K) cloud with $\sim 10^5$ $M_\odot$ becomes gravitationally unstable at $\rho \sim 10^{-20}$ g cm^{-3} and collapses. Based on this, we set the central density and temperature of the cloud to $\rho_c = 1.67 \times 10^{-20}$ g cm^{-3} and $T = 8000$ K, giving a mass and radius of 1.17×10^5 $M_\odot$ and 10.8 pc, respectively. Although we here do not impose an external FUV radiation, H_2 is collisionally dissociated for $\rho \gtrsim 10^{-20}$ g cm^{-3} and $T \gtrsim 6000$ K. Note that we neglect the dark-matter gravity since the cloud is already bound by the self-gravity of its gas. Our simulation box size is (50 pc)^3 and refinement is controlled by insisting that one Jeans length is resolved by at least 64 grid cells (e.g. Turk et al. 2012). Under this condition, the simulation uses 23 out of the allowed 25 refinement levels, ensuring we are resolved by the above criteria at all times and giving a limiting resolution of $\lesssim 0.1$ au.

The development of turbulence in the central region of forming first galaxies has been suggested by numerical simulations (e.g. Wise & Abel 2007; Greif et al. 2008). In the initial phase of collapse with $\sim 10^{-20}$ g cm^{-3}, the turbulence is still subsonic in the cloud. To consider the density and velocity perturbations due to the turbulence, we initially impose a subsonic velocity field (the root mean square of the velocity is set to $0.1 c_s$) with power spectrum $P(k) \propto k^{-4}$, which corresponds to the so-called Larson's law for the contemporary star-forming regions (Larson 1981). To ensure that the turbulence is adequately resolved, we select the maximum k-mode value of 1/10 of the number of cells across the cloud.

We consider the non-equilibrium primordial chemistry of 9 species (H, H_2, e^-, H^+, H_2^+, H^-, He, He^+, and He^{++}) and 13 hydrogen reactions selected to reproduce the correct thermal/chemical evolution of the warm atomic-cooling cloud (reactions 3, 4, 7–10, 12, 15–18, 28, and 32 in table 2 of Omukai 2001). We adopt the reaction rate coefficients updated by the following studies: 7–10 (Coppola et al. 2011), 15 (Martin, Schwarz & Mandy 1996), 17 (Stibbe & Tennyson 1999), and 28 (Ferland et al. 1992). The four helium reactions originally included in ENZO are also present, although they are not relevant in our calculation. We initially assume a uniform distribution of ionization degree with 10^{-4} and H_2 molecular fraction with 10^{-7}, respectively (e.g. Shang et al. 2010). At high density, the chemical reactions proceed faster than the cloud collapse and chemical equilibrium is achieved. To smoothly connect the non-equilibrium chemistry to that of equilibrium, we solve the chemical network including both the forward and reverse reactions for dominant processes. To solve the chemistry equations, we employ the piecewise exact solution method (Inoue & Inutsuka 2008) instead of the original ENZO solver, which cannot follow the chemical evolution with high enough density to reach the chemical equilibrium. For the radiative cooling, we consider atomic cooling (H Lyα, two-photon emission, and H^- free–bound, free–free emission) and H_2 cooling (rovibrational line and collision-induced emission). We also include the suppression of the cooling rate in the optically thick case by using the optical depth estimated as $\rho \kappa L_c$ (e.g. Omukai 2001; Shang et al. 2010), where κ includes the H_2-line opacity and the Rosseland mean opacity considering the H Rayleigh scattering, the H_2 collision-induced absorption, and the H^- bound-free and free–free absorption, and L_c the size of the central core, which is approximately given by the Jeans length for the spherically symmetric cloud in the runaway collapse. Finally, note that we do not include the heating/cooling associated with the chemical reactions because their effect is negligible during the thermal evolution of the atomic-cooling clouds.

3 RESULTS

Fig. 1 shows the density distribution at the end of the simulation, where the central density reaches $\sim 10^{-7}$ g cm^{-3}, for four different spatial scales; from the top-left clockwise, large-scale gas distribution ($\sim$1 pc), the collapsing core ($\sim$0.1 pc), the central $\sim$100 au region, and the protostar formed at the centre ($\sim$10 au). The central portion of the cloud undergoes the runaway collapse. The turbulence forms filamentary structures that channel material into the central region ($\rho \sim 10^{-8}$ g cm^{-3}), feeding the protostar. The left-bottom panel presents the density distribution around the protostar. At the end of this simulation, the protostellar mass reaches $\simeq 1$ $M_\odot$ and its radius $\simeq 2$ au. These values are consistent with the result of the stellar-structure calculation by Hosokawa et al. (2012), who assumed a steady and spherical accretion.

Fig. 2 shows the evolution of mass-weighted radial profiles of (a) density, (b) temperature, and (c) H_2 fraction. During collapse,

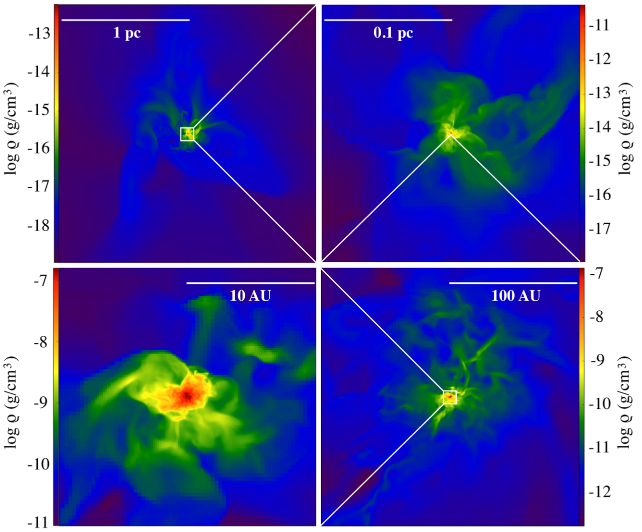

Figure 1. Density distribution in the plane through the density peak for four spatial scales: from top-left, clockwise: the large-scale gas distribution ($\sim$1 pc), a collapsing core by the H^- free–bound continuum cooling ($\sim$0.1 pc), the central region around the protostar ($\sim$100 au), and the final protostar ($\sim$10 au).

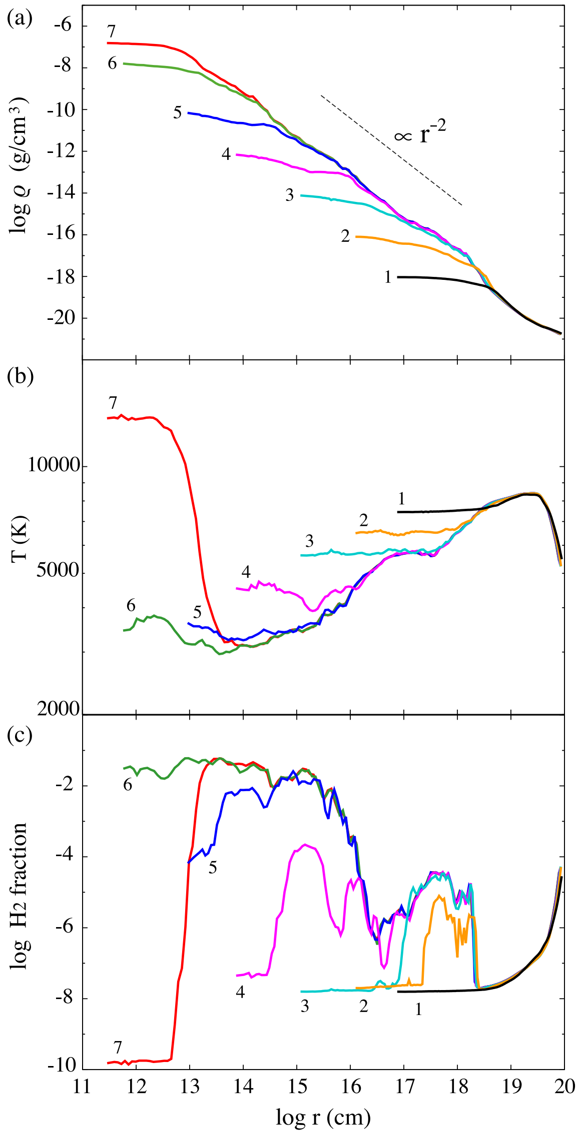

Figure 2. Mass-weighted radial profiles at different evolutionary stages of (a) mass density, (b) temperature, and (c) H_2 fraction. The time sequences are indicated by numbers: (1) 8.0 × 10^5 yr after the initial state of our simulation. (2) 9.3 × 10^4 yr after (1): the main coolants are the Lyα and two-photon emissions. (3) 1.6 × 10^4 yr after (2): dominant cooling process shifts to the H^- free–bound emission in the central core. (4) 1.8 × 10^3 yr after (3): H_2 formation via the three-body reaction becomes active at the centre. (5) 2.8 × 10^2 yr after (4): the cloud becomes optically thick to dominant H_2 lines. (6) 1.8 × 10^1 yr after (5): the cloud becomes optically thick to the continuum opacities and a hydrostatic core is formed at the centre. (7) 1.2 yr after (6): the final state of the simulation.

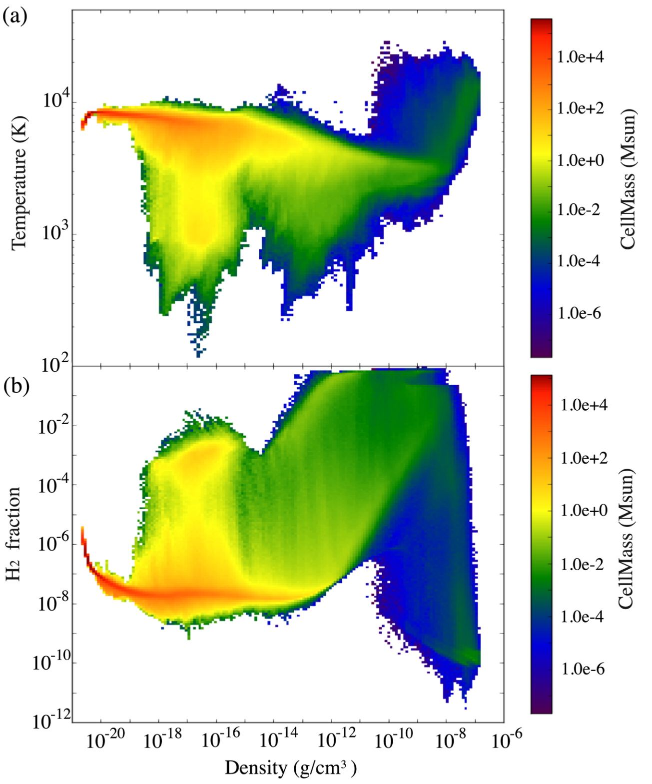

Figure 3. Phase diagrams showing the distribution of (a) density–temperature and (b) density–H_2 fraction of the collapsing cloud at the end of the simulation. The colours represent the total mass at the respective density and temperature.

the density profile obeys the self-similar solution, which consists of the central core with flat density distribution and envelope with the $\rho \propto r^{-2}$ law (e.g. Larson 1969). The central core collapses almost isothermally until $\sim 10^{-8}$ g cm^{-3} keeping the temperature at ∼5000 K. In the low-density regime of $\rho < 10^{-16}$ g cm^{-3}, the cooling is mainly via the H Lyα and two-photon emission. At higher density, the dominant cooling process shifts to the H^- free–bound emission ($H + e^- \rightarrow H^- + \gamma$). For $\gtrsim 10^{-9}$ g cm^{-3}, photons from the H^- free–bound emission are self-absorbed, as well as Rayleigh scattered by H. The gas cools further by the H^- free–free emission ($H + e^- \rightarrow H + e^- + \gamma$) until $\gtrsim 10^{-8}$ g cm^{-3}. Finally, the cloud becomes opaque to all those continuum opacities at $\sim 10^{-8}$ g cm^{-3} and a hydrostatic core, i.e. a protostar, with its mass $\simeq 0.2$ $M_\odot$ and radius $\simeq 1$ au is formed at the centre, where the core temperature is ∼4000 K. As the protostar grows to ~ 1 $M_\odot$, the temperature inside the protostar adiabatically increases to $\sim 10^4$ K.

The mass-weighted H_2 fraction initially approaches the equilibrium value ($\sim 10^{-8}$), where the formation through the electron-catalysed reaction ($H + e^- \rightarrow H^- + \gamma$; $H^- + H \rightarrow H_2 + H$) and the collisional dissociation ($H_2 + H \rightarrow 3H$) are balanced. At $\rho \gtrsim 10^{-13}$ g cm^{-3}, the H_2 fraction jumps up to ∼0.1 by the three-body reaction ($3H \rightarrow H_2 + H$) in the inner region ($r \lesssim 10^3$ au). However, neither the H_2-line nor collision-induced-emission (CIE) cooling plays a significant role in the thermal evolution: H_2 lines are optically thick for $\rho \gtrsim 10^{-10}$ g cm^{-3} and other continuum cooling is more important than the H_2 CIE cooling. After the protostar formation, the H_2 is dissociated inside owing to the high temperature.

Fig. 3 presents the phase diagrams showing the distribution of (a) temperature and (b) H_2 fraction as a function of the density at the end of the simulation. The cloud consists of two thermal phases of the gas, i.e. hot ($\sim$several 10^3 K) and cold ($\sim 10^3$ K) components. As seen in Figs 2(b) and 3(a), most of the collapsing gas resides in the hot component, which ultimately forms a protostar at the centre. Note that since the density profile follows the self-similar form during the runaway collapse and thus the radial position has one-to-one correspondence with the density (Fig. 2a), the density–temperature distribution of the hot component is just a reflection of the temperature profile (Fig. 2b). The H_2 fraction in the hot component remains almost constant at $\sim 10^{-8}$ up to 10^{-13} g cm^{-3} and then increases almost proportionally to the density for higher density by

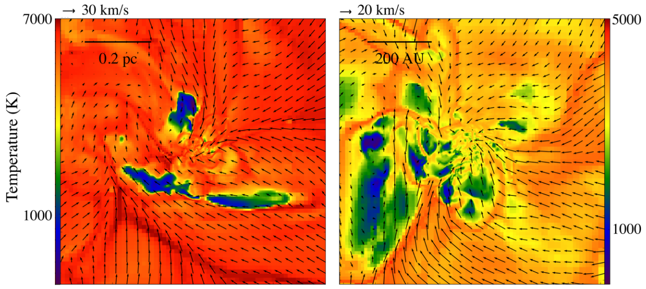

Figure 4. Temperature (colour) and velocity field (arrows) in the plane through the density peak for two spatial scales. Cold regions are formed by the chemothermal instabilities due to the H_2 formation by the electron-catalysed reaction (left) and by the three-body reaction (right).

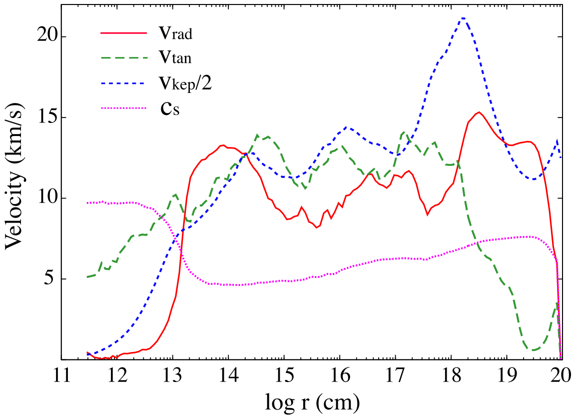

Figure 5. Profiles of the radial (solid) and tangential velocities (long-dashed) at the end of the simulation. For comparison, a half of the Keplerian velocity (short-dashed) and sound speed (dotted) are also shown. All the quantities are spherically averaged.

the three-body reaction until finally dissociated at $\gtrsim 10^{-8}$ g cm^{-3} as a result of the protostar formation.

Meanwhile, the cold component exists over the wide density range, $10^{-18} \lesssim \rho \lesssim 10^{-11}$ g cm^{-3}. This gas is produced by the thermal instability induced by the combination of the adiabatic cooling due to the turbulent expansion and the subsequent H_2 cooling. Once the temperature decreases via adiabatic cooling, the H_2 dissociation becomes inefficient, enhancing the H_2 fraction and its cooling rate, causing the temperature to plummet. This process is known as the chemothermal instability associated with the H_2 formation/dissociation (Yoshii & Sabano 1979; Silk 1983).

Fig. 4 presents the temperature distribution and velocity fields for two different scales. In both panels, the coexistence of the cold and hot components is clearly visible. Turbulence establishes a complex structure of interacting shocks and stagnation points. The cold components in the two scales are produced by the thermal instabilities due to the H_2 formation through the electron-catalysed reaction (∼0.2 pc) and three-body reaction (∼200 au), see also Fig. 3(b). The cold components are not massive enough to be gravitationally bound and have no influence on the evolution of the central collapsing region.

Fig. 5 presents the profiles of the radial and tangential velocities. Also shown for comparison is half of the Keplerian velocity and the sound speed. Both the radial and tangential flows become supersonic with the Mach number of 2–3. At the surface of the protostar, the radial flow is abruptly brought to a halt. In the accreting envelope, the tangential velocity is as large as half the Keplerian velocity, in accordance with previous studies of Pop III star formation (e.g. Abel, Bryan & Norman 2002; Yoshida, Omukai & Hernquist 2008). It is known that the cloud can contract in the runaway fashion even with conserved angular momentum as long as the temperature does not increase with the density (e.g. Narita, Hayashi & Miyama 1984; Saigo & Hanawa 1998). We note that the turbulent velocity is accelerated to the well-known universal value of $\sim 0.5\, v_{\rm Kep}$ soon after the gravitational collapse starts even with initially weak turbulence. Thus, the result seems unlikely to depend on the initial turbulent velocity. After protostar formation, on the other hand, materials initially located in the outer radius and thus with higher specific angular momentum begin to fall in, and the centrifugal radius increases outwards (Saigo, Matsumoto & Hanawa 2000). In our simulation, however, the rotationally supported disc has not yet appeared because the centrifugal radius ($\lesssim$0.1 au; McKee & Tan 2008) is still smaller than the stellar radius ∼1 au in this early accretion phase.

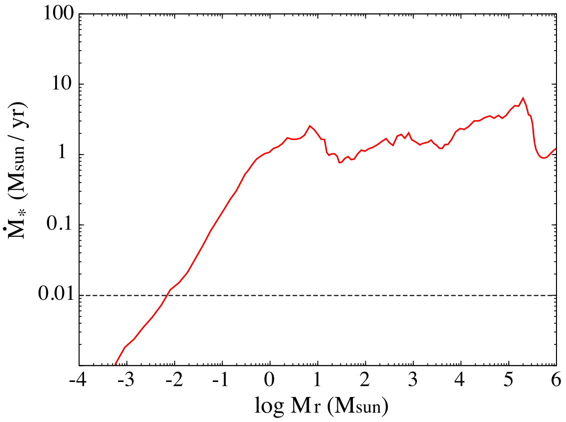

Figure 6. Profile of the mass infall rate ($\dot{M}_* = -4\pi\rho r^2 v_{\rm rad}$) as a function of the enclosed mass at the end of the simulation. The horizontal line indicates the critical value 10^{-2} M$_\odot$ yr^{-1}, above which the protostar swells to supergiant and the radiative feedback is strongly suppressed. (Hosokawa et al. 2012).

Fig. 6 shows the radial profile of the mass infall rate as a function of the enclosed mass. This can be regarded as the temporal evolution of the accretion rate after the protostar formation. Note that the value inside the protostar ($M_{\rm r} \lesssim 1$ M$_\odot$) is not equivalent to the accretion rate. The infall rate becomes almost constant for the flat temperature profile because in the self-similar solution, the flat temperature profile is proportional to $c_{\rm s}^3/G$, which depends only on the temperature of the accreting envelope. The typical value is as high as ∼2 M$_\odot$ yr^{-1}, which is consistent with the previous simulations starting from the cosmological initial condition (e.g. Latif et al. 2013b). This infall rate is larger than $20c_{\rm s}^3/G$ for $T = 8000$ K and similar to the value found for the runaway collapse starting from an initial condition not so far from the hydrostatic equilibrium. (Foster & Chevalier 1993). The protostar is expected to grow via such rapid accretion to an SMS within its lifetime $\sim 10^6$ yr. When the stellar mass exceeds $\sim 10^5$ M$_\odot$, the SMS is expected to collapse to a BH by the general relativistic instability (Chandrasekhar 1964; Hosokawa et al. 2013).

4 CONCLUSION AND DISCUSSION

We simulated the collapse of a massive ($\gtrsim 10^5$ M$_\odot$) and warm (∼8000 K) primordial-gas cloud using idealized initial conditions with a weakly turbulent field. We found that the cloud collapses nearly isothermally through H-atomic cooling and does not undergo a major episode of fragmentation, despite the inclusion of turbulence. Finally, a small protostar with mass $\sim$0.2 $\mathrm{M}_{\odot}$ is formed when the central part becomes optically thick to the continuum radiation at $\rho \gtrsim 10^{-8}$ g cm^{-3} and grows to the mass $\simeq$1 $\mathrm{M}_{\odot}$ and radius $\simeq$2 au by the end of the simulation.

Once formed, the protostar grows via rapid accretion from the dense filamentary flows at an approximately constant rate $\sim$2 $\mathrm{M}_{\odot}\ \mathrm{yr}^{-1}$. Where the accretion rate is higher than 10^{-2} $\mathrm{M}_{\odot}\ \mathrm{yr}^{-1}$ (dashed line in Fig. 6), the protostar is known to develop a giant-like structure with a bloated stellar envelope and contracting central core (Hosokawa et al. 2012, 2013) and grows while avoiding the significant mass-loss due to the stellar pulsation (Inayoshi et al. 2013). Since the effective temperature of such a supergiant protostar is $\lesssim 10^4$ K, the UV feedback is unlikely to prevent the mass accretion on to the star. However, recent simulation by Regan, Johansson & Haehnelt (2014) suggests the possibility of disc fragmentation around the protostar. Further simulations of the disc and the fragments with proper treatment of the H2-line cooling are needed to see whether such a high accretion rate continues to be maintained. After the protostar grows to an SMS ($\gtrsim 10^5$ $\mathrm{M}_{\odot}$) via rapid accretion, it eventually collapses through the general relativistic instability to turn into a seed of high-z SMBHs (e.g. Mortlock et al. 2011).

In this Letter, we started the calculation from the initial condition of a critical BE sphere with turbulence, and found a single protostar formed without a major episode of fragmentation. Since at $\lesssim$0.1 pc the profiles of the density and tangential velocity converge to self-similar forms with $\rho \propto r^{-2}$ and $v_{\mathrm{tan}} \simeq 0.5\, v_{\mathrm{Kep}}$, independent of the initial conditions (Figs 2 a and 5), we expect that our conclusions depend only weakly on the initial setup. To confirm this speculation, we need to investigate the dependence on the initial conditions. In particular, strong turbulence could prompt the efficient fragmentation, instead of forming a single SMS (e.g. Clark et al. 2011). Similarly, SMS formation from the proper cosmological initial condition remains to be explored for future studies.

In this simulation, we have neglected the effect of magnetic fields. Previous studies suggest that magnetic field strength could rival that of the turbulent energy (e.g. Federrath et al. 2011; Turk et al. 2012; Latif et al. 2013a) with the effect of either increasing accretion efficiency (via magnetic breaking producing a more spherical flow) or decreasing it via protostellar jets (Machida et al. 2006). This exploration will be left for future investigations.

ACKNOWLEDGEMENTS

We thank the ENZO and YT support teams, especially Brian O'Shea and Matthew Turk, for their useful advice. We also thank Takashi Nakamura, Takashi Hosokawa, Naoki Yoshida, Shu-ichiro Inutsuka, Tsuyoshi Inoue, and Kei Tanaka for their fruitful discussions. The results are analysed using the visualization toolkit for astrophysical data YT (Turk et al. 2011). Numerical computations were carried out on Cray XC30 at the Center for Computational Astrophysics of the National Astronomical Observatory of Japan. This work is supported in part by the grants-in-aid by the Ministry of Education, Culture, and Science of Japan (KI 23·838; KO 21684007, 25287040)

REFERENCES

Abel T., Bryan G. L., Norman M. L., 2002, Science, 295, 93
Begelman M. C., Volonteri M., Rees M. J., 2006, MNRAS, 370, 289
Bromm V., Loeb A., 2003, ApJ, 596, 34
Bryan G. L. et al., 2014, ApJS, 211, 19
Chandrasekhar S., 1964, ApJ, 140, 417
Choi J.-H., Shlosman I., Begelman M. C., 2013, ApJ, 774, 149
Clark P. C., Glover S. C. O., Klessen R. S., Bromm V., 2011, ApJ, 727, 110
Coppola C. M., Longo S., Capitelli M., Palla F., Galli D., 2011, ApJS, 193, 7
Di Matteo T., Khandai N., DeGraf C., Feng Y., Croft R. A. C., Lopez J., Springel V., 2012, ApJ, 745, L29
Fan X., 2006, New Astron. Rev., 50, 665
Federrath C., Sur S., Schleicher D. R. G., Banerjee R., Klessen R. S., 2011, ApJ, 731, 62
Ferland G. J., Peterson B. M., Horne K., Welsh W. F., Nahar S. N., 1992, ApJ, 387, 95
Foster P. N., Chevalier R. A., 1993, ApJ, 416, 303
Greif T. H., Johnson J. L., Klessen R. S., Bromm V., 2008, MNRAS, 387, 1021
Hosokawa T., Omukai K., Yorke H. W., 2012, ApJ, 756, 93
Hosokawa T., Yorke H. W., Inayoshi K., Omukai K., Yoshida N., 2013, ApJ, 778, 178
Inayoshi K., Omukai K., 2011, MNRAS, 416, 2748
Inayoshi K., Omukai K., 2012, MNRAS, 422, 2539
Inayoshi K., Hosokawa T., Omukai K., 2013, MNRAS, 431, 3036
Inoue T., Inutsuka S.-i., 2008, ApJ, 687, 303
Larson R. B., 1969, MNRAS, 145, 271
Larson R. B., 1981, MNRAS, 194, 809
Latif M. A., Schleicher D. R. G., Schmidt W., Niemeyer J., 2013a, MNRAS, 432, 668
Latif M. A., Schleicher D. R. G., Schmidt W., Niemeyer J., 2013b, MNRAS, 433, 1607
Machida M. N., Omukai K., Matsumoto T., Inutsuka S.-i., 2006, ApJ, 647, L1
McKee C. F., Tan J. C., 2008, ApJ, 681, 771
Martin P. G., Schwarz D. H., Mandy M. E., 1996, ApJ, 461, 265
Mortlock D. J. et al., 2011, Nature, 474, 616
Narita S., Hayashi C., Miyama S. M., 1984, Prog. Theor. Phys., 72, 1118
Omukai K., 2001, ApJ, 546, 635
Regan J. A., Haehnelt M. G., 2009, MNRAS, 396, 343
Regan J. A., Johansson P. H., Haehnelt M. G., 2014, MNRAS, 439, 1160
Saigo K., Hanawa T., 1998, ApJ, 493, 342
Saigo K., Matsumoto T., Hanawa T., 2000, ApJ, 531, 971
Shang C., Bryan G. L., Haiman Z., 2010, MNRAS, 402, 1249
Silk J., 1983, MNRAS, 205, 705
Stibbe D. T., Tennyson J., 1999, ApJ, 513, L147
Turk M. J., Smith B. D., Oishi J. S., Skory S., Skillman S. W., Abel T., Norman M. L., 2011, ApJS, 192, 9
Turk M. J., Oishi J. S., Abel T., Bryan G. L., 2012, ApJ, 745, 154
Wise J. H., Abel T., 2007, ApJ, 665, 899
Wise J. H., Turk M. J., Abel T., 2008, ApJ, 682, 745
Yoshida N., Omukai K., Hernquist L., 2008, Science, 321, 669
Yoshii Y., Sabano Y., 1979, PASJ, 31, 505

This paper has been typeset from a TEX/LATEX file prepared by the author.